Title
Anion-exchange membrane water electrolysis: insights from round-robin testing

Journal
Frontiers in Energy Research, 14

ISSN
2296-598X

Authors
Kreider, Melissa E
Mendoza, B Milenia Rojas
Brusse, Luke
et al.

Publication Date
2026-06-12

DOI
10.3389/fenrg.2026.1794912

frontiers in Energy Research

TYPE Methods
PUBLISHED 12 June 2026
DOI 10.3389/fenrg.2026.1794912

OPEN ACCESS

EDITED BY
Ellen B. Stechel,
Arizona State University, United States

REVIEWED BY
Schwan Hosseiny,
CENmat, Germany
Silvia Barbi,
University of Modena and Reggio Emilia, Italy

*CORRESPONDENCE
Melissa E. Kreider,
melissa.kreider@nlr.gov

†These authors have contributed equally to this work

RECEIVED 23 January 2026
REVISED 12 March 2026
ACCEPTED 04 May 2026
PUBLISHED 12 June 2026

CITATION
Kreider ME, Rojas Mendoza BM, Brusse L, Syar D, Kwak M, Yang P, Chang H-MJ, Hannagan RT, Rios Amador I, Ekennia AC, Oliveira NJ, Nielander AC, Boettcher SW, Zenyuk IV, Jaramillo TF, Alia SM and Lakshmanan B (2026) Anion-exchange membrane water electrolysis: insights from round-robin testing.
Front. Energy Res. 14:1794912.
doi: 10.3389/fenrg.2026.1794912

Anion-exchange membrane water electrolysis: insights from round-robin testing

Melissa E. Kreider[1]*†, B. Milenia Rojas Mendoza[2,3†], Luke Brusse[4], Duha Syar[5], Minkyoung Kwak[5], Patrick Yang[6], Hung-Ming Joseph Chang[6], Ryan T. Hannagan[2], Isabela Rios Amador[2,3], Anthony C. Ekennia[5], Nicholas J. Oliveira[7], Adam C. Nielander[3], Shannon W. Boettcher[5], Iryna V. Zenyuk[6], Thomas F. Jaramillo[2,3], Shaun M. Alia[1] and Balasubramanian Lakshmanan[4]

[1]Chemistry and Nanoscience Center, National Laboratory of the Rockies, Golden, CO, United States, [2]Department of Chemical Engineering, Stanford University, Stanford, CA, United States, [3]SUNCAT Center for Interface Science and Catalysis, SLAC National Accelerator Laboratory, Menlo Park, CA, United States, [4]Versogen, Newark, DE, United States, [5]Department of Chemical and Biomolecular Engineering and Department of Chemistry, University of California, Berkeley, Berkeley, CA, United States, [6]Department of Chemical and Biomolecular Engineering, National Fuel Cell Research Center, University of California Irvine, Irvine, CA, United States, [7]Nel Hydrogen, Wallingford, CT, United States

As research and industrial interest in anion-exchange membrane water electrolysis (AEMWE) grows, there is an increasing need for reliable baselines and cross-lab validation of results. The wide variety of material sets and operating conditions under consideration for AEMWE has thus far limited efforts for standardization. In this study, round-robin testing was conducted in deionized water and KOH-based supporting electrolyte by 5 institutions from academia, national laboratories, and industry to provide baseline performance data and identify sources of cross-lab variability. Baseline membrane electrode assemblies were fabricated with commercial catalysts, membranes, and transport layers using standard techniques and tested using reagent-grade electrolytes, aiming for accessibility rather than state-of-the-art performance. From all tests, the average voltage at 1 A/cm^2 was 2.72 $\pm$ 0.17 V and 1.87 $\pm$ 0.03 V in deionized water and 0.1 M KOH, respectively. The maximum in-house and cross-lab variations at this current density were 118 mV and 476 mV in water and 60 and 88 mV in 0.1 M KOH. The KOH purity, station contamination, and temperature control were identified as possible factors affecting performance between labs, with in-house specific variation attributed to sample-to-sample differences in fabrication, cell assembly, and station contamination. This work provides a commercial baseline for the field and highlights the need for improved standardization and reproducibility in AEMWE research.

KEYWORDS
anion-exchange membrane water electrolysis, benchmarking, hydrogen, round robin, water electrolysis

1 Introduction

Anion-exchange membrane water electrolysis (AEMWE) has recently gained significant attention as a pathway for low-cost, scalable hydrogen production

(Du et al., 2022; Varcoe et al., 2014). Despite rapid growth in academic and industrial interest, the field lacks consistent benchmarking practices. Reports often vary widely in catalyst loading, ionomer content, cell hardware, electrolyte purity, operating temperature, and measurement protocol, making it difficult to compare results across studies or assess technological progress (Huang et al., 2020; Hassan et al., 2023; Lim et al., 2024; Titheridge et al., 2024). A major source of this variability is the absence of standardization; without standardized protocols, researchers cannot determine whether performance differences arise from intrinsic material properties or from differences in fabrication, operating conditions, or measurement infrastructure (Lee et al., 2022; Meek et al., 2019; Miller et al., 2020; Xu et al., 2022). This gap leaves the AEMWE community without a shared reference point to support reproducibility studies and technology validation for cross-lab comparison.

In the more technologically mature proton-exchange membrane (PEM) and liquid-alkaline (LA) water electrolysis fields, several efforts have been undertaken to develop standard protocols (Tomić et al., 2023) and evaluate performance across laboratories (Tomić et al., 2023; Bender et al., 2019; Appelhaus et al., 2024; Parimuha et al., 2025). Although differences in materials and test protocols remain, these efforts have been facilitated by some agreement in the field on the baseline catalysts, membranes, and operating conditions (Danilovic et al., 2021). As a hybrid between PEM and LA, AEMWE has a wide spectrum of design options regarding platinum-group metal (PGM) catalysts, electrode fabrication methods, supporting electrolyte, and target current densities. These choices have a significant impact on performance and there is currently no consensus in the field. For example, both deionized (DI) water and supporting electrolyte environments are widely used in the literature, with little agreement on which approach is most commercially viable (Hassan et al., 2022; Zhang et al., 2023). DI operation reduces balance-of-plant cost, minimizes corrosion of metal components, and avoids the handling requirements associated with caustic electrolytes. In contrast, supporting electrolytes such as potassium or sodium hydroxide, bicarbonate, and carbonate at concentrations from 1 mM to 1 M enhance ionic conductivity, reduce transport losses, and often improve electrochemical stability. However, they also introduce challenges related to electrolyte cost, concentration maintenance, hardware corrosion, and shunt currents (Ayers et al., 2019; Zeng and Zhang, 2010).

This work aims to establish a framework that supports more consistent and interpretable comparisons across the field by identifying performance differences between laboratories, evaluating in-house reproducibility, and determining the variables that most influence AEMWE behavior. A comparison of AEMWE measurements from the literature using nominally similar catalysts and test conditions is shown in Figure 1. Despite these similarities, large variations remain in catalyst loading (0.3–5 mg/cm^2 for anodes, 0.3–1 mg/cm^2 for Pt); membrane chemistry (PiperION, Sustainion, Fumasep); membrane thickness (30–80 μm); porous transport layer (Ni, stainless steel, platinized Ti); cell temperature (50 °C–80 °C); and KOH concentration (0.5–1 M KOH) that make direct comparison of the results across laboratories difficult. The reported current densities at 1.8 V vary from 0.5 to 1.55 A/cm^2. For those tests that reach 1 A/cm^2, the spread in voltages at that current density is 115 mV. This performance disparity may be attributable to the noted differences in the membrane electrode assembly (MEA) and test conditions or to other, unidentified differences in cell hardware and test stand design that affect performance.

While AEMWE is not at a stage where specific materials or operating conditions should be prescribed, a benchmarking effort must make choices on what tests are relevant and helpful to the field. Here, baseline materials, operating conditions, and test protocols are selected to maximize accessibility and reproducibility. Commercial catalysts, transport layers, and membranes with demonstrated durability are used to ensure consistent MEA fabrication. For the cathode, the most common catalysts are Pt- or Ni-based; here, Pt/C was chosen due to its commercial availability and improved stability. For the anode, NiFe- and Co-based catalysts have largely replaced IrO_2 due to their low cost and comparable activity; here, Co_3O_4 is chosen because of its improved stability, particularly in water. Because electrolyte choice has a large effect on performance and emphasizes different aspects of device behavior, this study evaluates AEMWE performance under both 0.1 M KOH and DI conditions. Reagent-grade KOH is used for accessibility and relevance to the industrial application. The 0.1 M concentration is chosen to minimize corrosion of stainless steel components in the test stations and cell hardware, while providing sufficient ionic conductivity to be reflective of performance and durability in supporting electrolyte. Operating conditions such as temperature and voltage/current density are chosen to be compatible with these materials and representative of typical literature practices. Due to the chemical incompatibility of many commercial PEMWE hardware components with alkaline electrolytes, custom-built AEMWE hardware is employed for internal consistency, and performance is compared across additional hardware designs to evaluate hardware-dependent effects. Electrochemical protocols, including short break-in periods and comprehensive beginning-of-test characterization using polarization curves and electrochemical impedance spectroscopy (EIS), are adapted from established PEM and bipolar membrane (BPM) electrolyzer procedures (Rios Amador et al., 2023). These coordinated choices provide a rigorous baseline dataset for benchmarking while avoiding implicit endorsement of specific components.

While several recent studies have proposed testing protocols and benchmarking approaches for AEMWE systems (Titheridge et al., 2024), most evaluations have been performed within a single laboratory (Tricker et al., 2023). In this work, we report a multi-laboratory, single-cell AEMWE round-robin study across five laboratories conducted by the National Laboratory of the Rockies (NLR), Stanford University/SLAC National Accelerator Laboratory, Versogen, the University of California–Berkeley (UCB), and the University of California–Irvine (UCI), with consultation from Nel Hydrogen. By comparing performance under both supporting-electrolyte and DI conditions, we quantify the expected voltage range at 1 A/cm^2 and identify possible contributors to in-house and cross-lab variability, including electrolyte purity, station contamination, temperature control, MEA fabrication differences, and cell assembly. We further make suggestions for test variables and performance metrics that should be reported for all studies to allow for meaningful comparison in the literature. While innovation in AEMWE is still needed, these efforts in standardization of testing

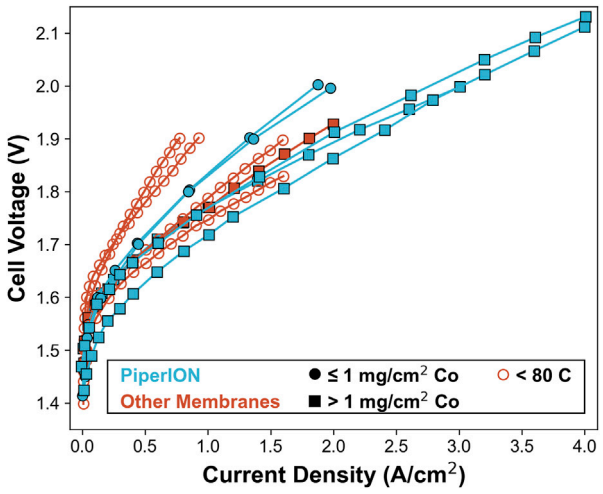

FIGURE 1
Comparison of literature AEMWE performance using Co_3O_4 anode and Pt/C cathode catalysts in KOH supporting electrolyte. The membrane type is shown by color, divided into PiperION (blue) and other anion-exchange membranes (orange), including Sustainion and Fumasep. Operation temperature below 80°C is denoted by open markers. Circle markers denote ≤1 mg/cm^2 and square markers denote > 1 mg/cm^2 Co loading in the anode. Data were digitized from published results (Tricker et al., 2024; Volk et al., 2023; Yanagi et al., 2025; Kreider et al., 2024; Tricker et al., 2023; Park et al., 2025; Ham et al., 2021; Wu and Scott, 2011; Kim et al., 2023).

and reporting are crucial to improving the reproducibility and reliability of the field.

2 Protocol scope

2.1 Scope and applicability

The purpose of this protocol is to provide a baseline for AEMWE single-cell performance in water and supporting electrolyte (Scheme 1). While not optimized, this protocol provides standard material sets, operating conditions, and electrochemical testing steps that may be used across labs for validation of test stands and novel materials. The findings about the magnitude and causes of in-house and cross-lab differences are applicable for all labs aiming to improve reproducibility.

2.2 Summary of method

The protocol describes the full process of single-cell AEMWE testing, from catalyst powders to electrochemical characterization. Protocols for both water and supporting electrolyte are provided. In brief, electrodes are fabricated via spraying of catalyst layers onto transport layers, and the membrane is ion exchanged. The MEA is assembled in the cell hardware, as shown in Figure 2. In the test stand, recirculating electrolyte is pumped into the cell, with cell heaters and/or electrolyte heaters used to reach the desired temperature, measured by thermocouples in the cell body and electrolyte. After a short break-in step, electrolyzer performance is assessed using polarization curves and EIS from low to high current density.

2.3 Health and safety warning

Appropriate personal protective equipment, including safety glasses, gloves, and lab coats, should be used. Catalyst nanomaterial powders should be handled in a fume hood until bound to a substrate. Electrolyte solutions should be prepared in a fume hood and handled with care. Proper sealing of the cell and test station components is needed to prevent leaks of generated hydrogen. Leaks from the cell and fittings can be assessed with a handheld hydrogen gas sensor. Electrolyzer testing can pose electrical hazards. Use properly certified power supplies or potentiostats with insulated cables. De-energize the cell before changing any electrical connections. Cell operation at 50 °C–80 °C will result in hot cell hardware. Allow hardware to cool prior to disassembly.

3 Procedure

See Supplementary Material for step-by-step protocol, photographs of each lab's test stand (Supplementary Figures S1-S5), and a summary of experimental differences between labs (Supplementary Table S1).

3.1 Materials

3.1.1 DI water

Commercial Co_3O_4 (US Research Nanomaterials Inc., 99%), Pt/C (5% Pt, Fuel Cell Store), stainless steel fiber porous transport layer (PTL) (25AL3, Bekaert), carbon gas diffusion layer (GDL) (Toray 120, Fuel Cell Store), PiperION-A TP85 membrane (40 µm, Versogen) and ionomer (5 wt% in ethanol), Milli-Q water (18.2 MΩ-cm), isopropanol (Fisher).

3.1.2 KOH

Commercial Co_3O_4 (US Research Nanomaterials Inc., 99%), Pt/C (47% Pt, TKK TEC10E50E), nickel fiber PTL (Currento 2Ni18-0.25, Bekaert), carbon GDL (AvCarb MGL280, 80,280-40), PiperION-A TP85 membrane (80 µm, Versogen) and ionomer (5 wt% in ethanol), Milli-Q water (18.2 MΩ-cm), n-propanol (Sigma Aldrich, OmniSolv, high-performance liquid chromatography grade), potassium hydroxide (reagent-grade, varying supplier and purity, details in Supplementary Table S1).

3.2 Electrode fabrication

3.2.1 DI water

The electrodes for DI testing were fabricated in a catalyst-coated substrate (CCS) configuration using a Sonotek Spray coater by Lab 4. The inks were prepared by adding 10 g water, 0.4 g ionomer solution, and 34 g isopropyl alcohol to 0.2 g Pt/C (for the cathodes) or 0.2 g Co_3O_4 (for the anodes). The mixture was transferred to a Falcon tube and bath-sonicated for a minimum of 2 h until the

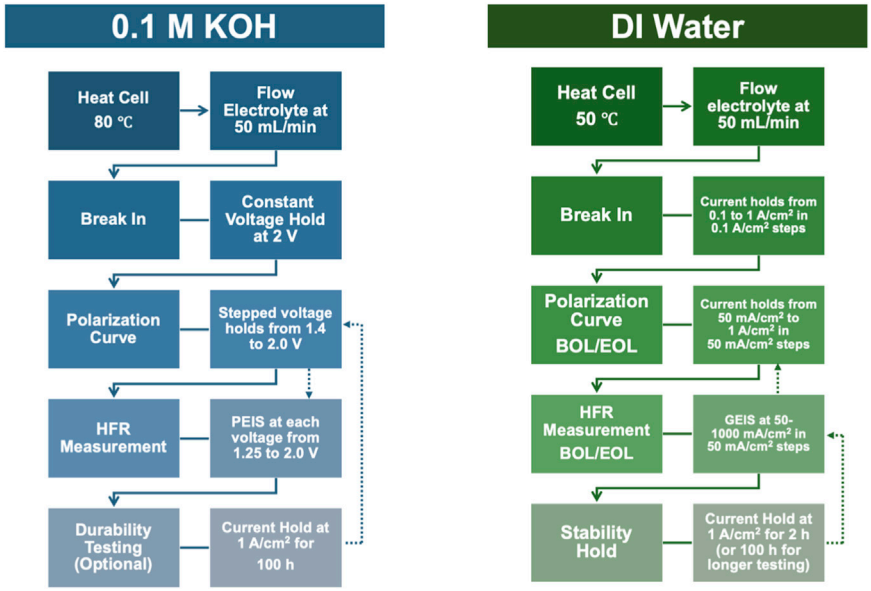

SCHEME 1
Flow chart of electrochemical testing procedure. Prior to electrochemical testing, the cell and electrolyte were heated until the internal cell temperature reached 80 °C for 0.1 M KOH experiments and 50 °C for DI water experiments. (Left) The protocol used for testing in 0.1 M KOH. The electrochemical sequence consisted of a break-in step (constant voltage hold at 2 V), followed by a polarization curve and HFR/EIS measurements collected at selected voltages. An optional stability hold at 1 A/cm^2 for 100 h was then conducted. (Right) The protocol used for testing in DI water operation. A different break-in procedure consisting of current holds from 0.1 to 1 A/cm^2 was used. Polarization curves were recorded with HFR/GEIS measurements performed at the same current densities. A stability hold at 1 A/cm^2 for 2 h was then conducted, followed by EOT impedance measurements and an EOT polarization curve. Further experimental details are provided in the Supplementary Material.

ink was fully dispersed. The PTL (anode) or GDL (cathode) was cut and taped onto the Sonotek spray coater hot plate (80 °C), with the front corners secured to ensure stability. The Sonotek settings were maintained at: shaping air 0.4 psi, flow rate 1, nozzle power 2, and line speed 60 mm/sec. Spraying was performed in a serpentine pattern to ensure full coverage. Loading was determined by weighing the electrodes; to weigh between sprays, the tape frame was removed, and the electrodes were allowed to cool to room temperature before weighing. This process was repeated until the desired loading was reached. After the catalyst was sprayed, a 2 wt% PiperION solution was applied over the catalyst layer in a pulsed serpentine pattern until the ionomer overlayer reached 10%–20% of the catalyst mass, for a total ionomer loading of 20%–30%. The final anode catalyst loading (including catalyst and ionomer) was 2.3–2.6 mg/cm^2. The total loading, including the Pt metal, the carbon support, and the ionomer, was 2.0 mg/cm^2 for the cathode. Unless otherwise specified, catalyst loadings are reported as total catalyst mass per geometric area (mg$_{cat}$/cm^2), while metal-only loadings (mg$_{metal}$/cm^2) are reported when determined by XRF.

3.2.2 KOH

The electrodes for supporting electrolyte testing were fabricated in a CCS configuration using an airbrush (Grex Tritium. TG3 Airbrush, 0.3 mm nozzle) by Lab 1. For the target loading of 0.8 mg$_{Co}$/cm^2 and 10 wt% ionomer, the anode ink was composed of 0.19 g Co_3O_4, 1.2 g water, 10.8 g n-propanol, and 0.42 g ionomer. For the target loading of 0.3 mg$_{Pt}$/cm^2 and 30 wt% ionomer, the cathode ink was composed of 0.15 g Pt/C, 6.8 g water, 6.4 g n-propanol, and 1.3 g ionomer. The inks were bath sonicated, using an ice bath to prevent overheating, and then horn sonicated for 1 min. 5 cm^2 PTLs and GDLs were taped to the vacuum hot plate (80 °C), using a thin PTFE backing sheet to prevent contamination of the hot plate. The electrodes were sprayed in a serpentine pattern, dispensing the full ink. After spraying, the catalyst metal loading was determined by X-ray fluorescence (XRF, Fischer XDV-SDD XRF).

3.3 Electrochemical testing

Prior to assembly, the membranes were ion exchanged according to manufacturer instructions, soaking in 0.5 M KOH for 1 h and repeating with fresh KOH. The cell hardware, custom-built by Versogen, consisted of Au-coated stainless steel flow fields with 5 cm^2 active area and single serpentine flow channels, Au-coated current collectors and stainless-steel endplates (Figure 2a). The cell contact resistance was measured to be 20 mΩ*cm^2. Testing by Lab 1 of their in-house hardware (Parimuha et al., 2025) compared to the shared hardware showed only small differences in performance (Supplementary Figure S6), indicating that the performance may be relatively insensitive to differences in hardware. PTFE gaskets were used to obtain the desired MEA compression of 30% and 20% for DI water testing and supporting electrolyte at torques of 50 in-lb and 40 in-lb, respectively. Details of the compression calculation are included in the SI. Rod heaters were inserted into each endplate, and cell temperature was monitored using a thermocouple inserted into the flow field. The standard protocol called for electrolyte

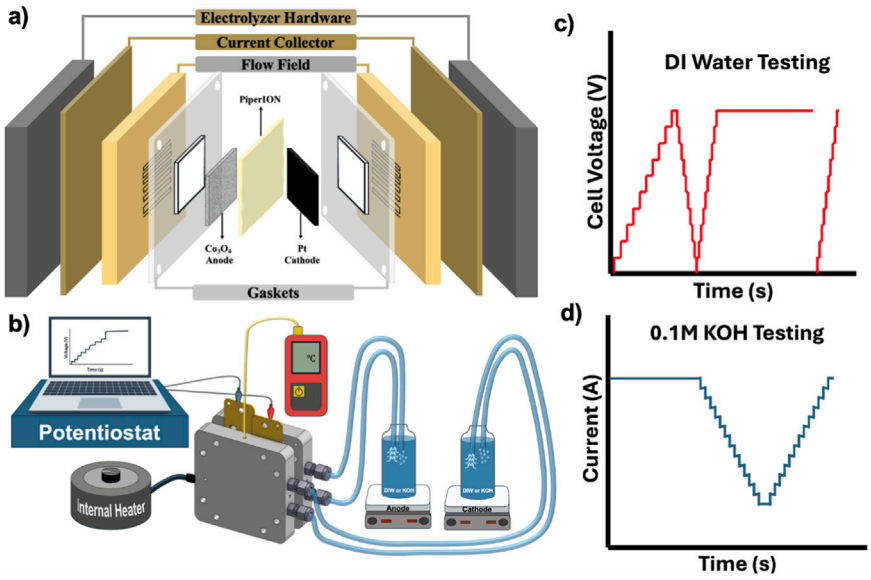

FIGURE 2
Schematic of round robin testing protocol. **(a)** Cell hardware design and MEA components. **(b)** Generalized test station set up, including cell and electrolyte heating. **(c)** Test sequence in DI water including break-in, BOT polarization curve, and short-term stability. Current was controlled and cell voltage was measured at each step. **(d)** Test sequence in 0.1 M KOH including break-in and BOT polarization curve. Cell voltage was controlled and current was measured at each step.

flow rates of 50 mL/min, recirculating from connected anode and cathode reservoirs, with preheating to deliver the electrolyte at the desired operation temperature, 50 °C or 80 °C for DI water and supporting electrolyte, respectively (Figure 2b). Deviations from this standard protocol for each lab are explained in detail in the Supplementary Material (Supplementary Figures S1-S5).

3.3.1 DI water

Once the cell temperature was stable, the MEA was conditioned and tested, as shown in Figure 2c. The conditioning protocol consisted of stepping the current up from 0.1 to 1 A/cm^2 in 2 min steps, holding at 1 A/cm^2 for 15 min, and then decreasing back to 0.05 A/cm^2 in 20 s steps. The next polarization curve, from 0.05 to 1 A/cm^2 in 0.05 A steps, held for 20 s each, was denoted as beginning of test (BOT). A series of galvanostatic electrochemical impedance spectroscopy (GEIS) scans were performed at fixed current densities of 0.1, 0.2, 0.3, 0.4, 0.5, 0.6, 0.7, 0.8, 0.9, and 1 A/cm^2, with superimposed alternating currents (AC) having magnitudes of 10% of each respective direct current (DC), up to a maximum of 0.05 A. A short-term stability test was conducted at 1 A/cm^2 for 2 h, and then the end of test (EOT) polarization curve and GEIS were measured. Details of the EIS measurements are given in Supplementary Table S2.

3.3.2 KOH

For testing in 0.1 M KOH, a slightly different conditioning and test protocol was used (Figure 2d). First, the cell was conditioned at 2 V for 2 h, using the high voltage to drive oxidation and reconstruction processes. Then, potentiostatic polarization curves were conducted from 2 V down to 1.4 V, and then back up to 2 V, all in 2 min steps. The polarization curve from 1.4 to 2 V was reported as the BOT. Next, potentiostatic EIS (PEIS) measurements were performed at the same voltages as the polarization curve with AC amplitude of 10 mV. 100 h durability tests at 1 A/cm^2 were also conducted, along with EOT polarization curves and EIS measurements. Details of the potentiostats and power supplies used by each lab are included in Supplementary Table S1. For a more detailed step-by-step procedure, refer to the Supplementary Material.

3.4 Data analysis

For each type of test, 4 sets of MEA components (electrodes, membrane, gaskets) were sent to each lab, along with the cell hardware provided by Lab 2. The results were reported as the average of triplicate measurements; in a few cases, as noted, only two replicates were measured. To compare performance, four main metrics were used. First, the current density at 2 V and the voltage at 1 A/cm^2 were evaluated as metrics of overall performance. Next, the high frequency resistance (HFR) was determined from the EIS at each voltage/current step (Supplementary Figure S7, details of the calculation method for each lab are given in the SI). At a high level, HFR was calculated either by fitting to a circuit model or interpolation to the intercept with the real impedance axis. The HFR-free voltage was further used to calculate the Tafel slope and kinetic voltage losses, allowing for separation of losses into ohmic (from HFR), kinetic (from Tafel fit), and mass transport (from residual) contributions. The average, in-house, and cross-lab variations in these metrics were compared. Error bars and tabulated error values for the overall values were calculated as the standard deviation of all measurements. In this work, variation refers to the quantitative spread in measured values (e.g., standard deviation

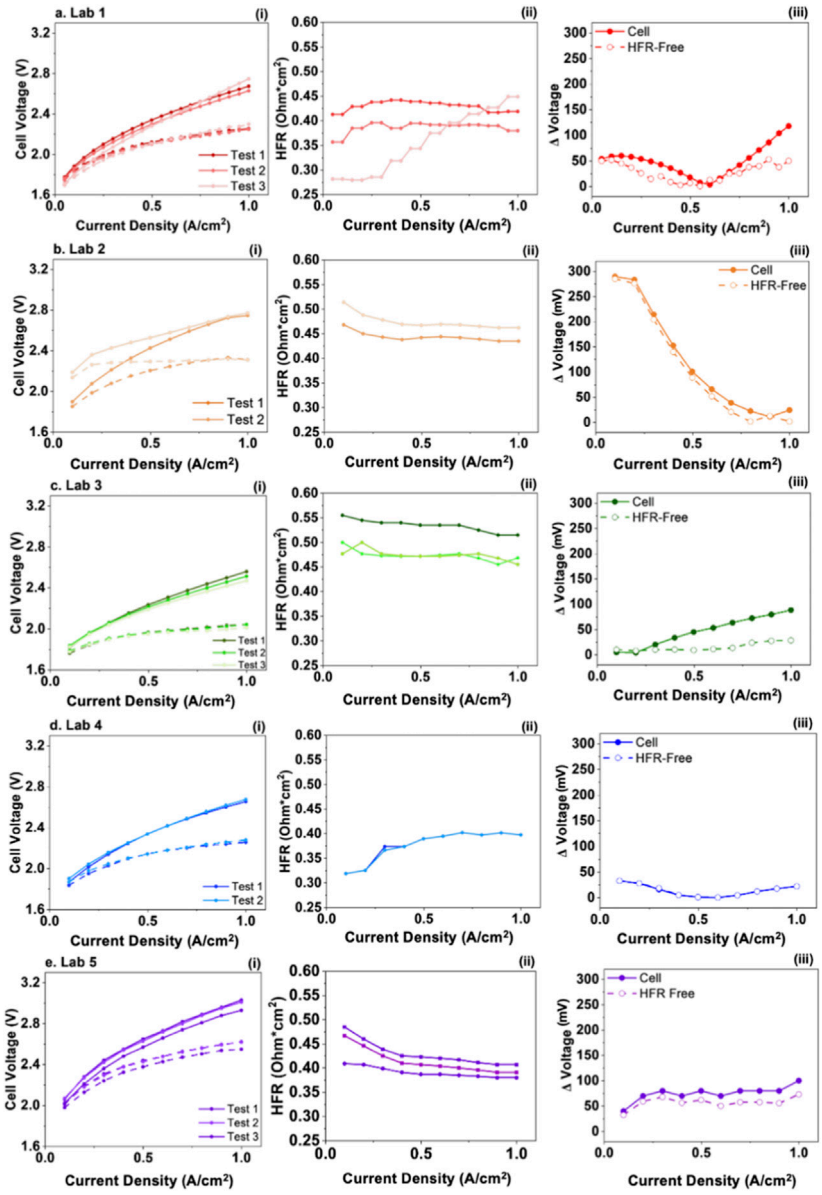

FIGURE 3
BOT performance in deionized water. **(i)** Full cell voltage (solid lines) and HFR-free (dashed lines) polarization curves, **(ii)** HFR values, and **(iii)** maximum cell (solid lines) and HFR-free (dashed lines) voltage variation in the triplicate as a function of current density for **(a)** Lab 1 (red), **(b)** Lab 2 (gold), **(c)** Lab 3 (green), **(d)** Lab 4 (blue), **(e)** and Lab 5 (purple). Three tests were reported for Labs 1, 3, and 5, while two were reported for Labs 2 and 4.

or max–min range, reported as ΔV), while variability refers to the qualitative reproducibility across repeats or laboratories.

4 Results

4.1 DI water

AEMWE operation in deionized water is attractive due to its simplified balance-of-plant, reduced corrosion of hardware components, and elimination of highly alkaline feeds. However, DI water also introduces significant ionic transport limitations due to its low ionic conductivity, leading to higher ohmic losses and lower overall cell performance relative to supporting electrolyte operation. The first half of the benchmarking effort, therefore, focused on DI water to evaluate reproducibility across the 5 labs. The MEA fabrication and test protocol are discussed in detail in the experimental section. All anodes were composed of a commercial Co_3O_4 catalyst layer with 2.3–2.6 mg/cm^2 loading and 10-20 wt% PiperION ionomer, supported on a stainless steel PTL. The cathode total catalyst loading was 2.0 mg/cm^2 with 10–20 wt% PiperION ionomer on a C GDL, and the membrane was 40 μm PiperION. Electrodes were fabricated at Lab 4 and distributed to the other labs.

Figure 3 shows the BOT performance for the triplicate experiments run by each lab in DI water. Labs 2 and 4 reported only two replicates; these results were not used to determine

TABLE 1 Performance summary in DI Water.

Lab	1*	2*,†	3*	4*,†	5*	Average^
Cell voltage at 1 A/cm^2 (V)	2.683 ± 0.049	2.758 ± 0.012	2.514 ± 0.036	2.666 ± 0.011	2.990 ± 0.043	2.72 ± 0.17
HFR (mΩ*cm^2) at 1 A/cm^2	412 ± 8	449 ± 11	480 ± 26	398 ± 1	393 ± 11	427 ± 37
HFR-free voltage at 1 A/cm^2 (V)	2.271 ± 0.044	2.310 ± 0.001	2.034 ± 0.013	2.269 ± 0.011	2.597 ± 0.041	2.30 ± 0.19

*Values were reported as the mean and standard deviation of replicates from each lab.
^Values were reported as the mean and standard deviation of replicates from all labs.
†Only two replicates.

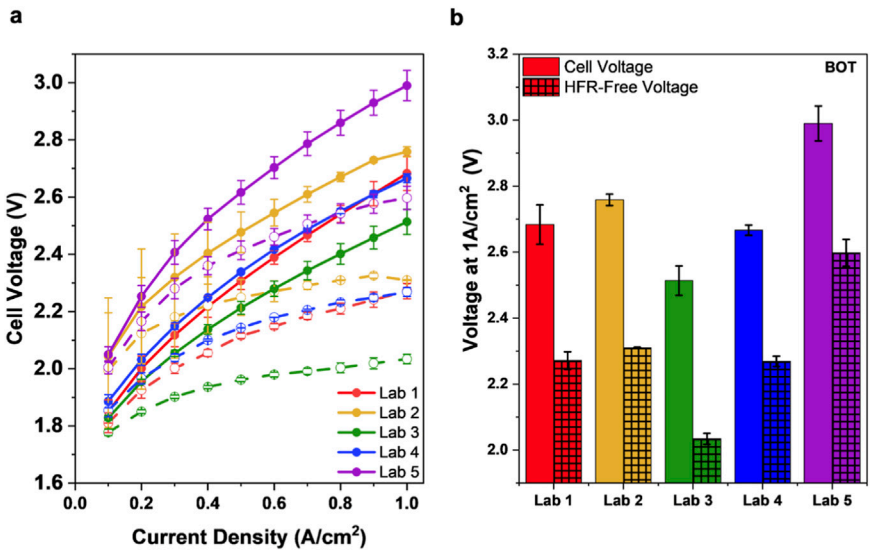

FIGURE 4
BOT performance in deionized water. **(a)** Full cell voltage (solid lines) and HFR-free (dashed lines) polarization curves for all laboratories. **(b)** Summary of full cell voltage (solid bars) and HFR-free voltage (patterned bars) at 1 A cm^{-2}. Colors correspond to Lab 1 (red), Lab 2 (gold), Lab 3 (green), Lab 4 (blue), and Lab 5 (purple). Data were reported as the average and standard deviation of tests performed in triplicate (duplicate for Labs 2 and 4).

minimum values of the standard deviation and maximum spread but were used in all other calculations. The performance for each lab is further summarized in Table 1. In each triplicate, significant variation was observed in both full cell and HFR-free polarization curves (Figures 3a–3ei), as well as the HFR values (Figures 3a–3eii). The HFR, which is sensitive to ionic conductivity and temperature (Ito et al., 2011), varied with current density and typically decreased or stabilized near ~0.5 A/cm^2. However, the magnitude and variation of HFR differed from lab to lab. To quantify in-house repeatability, we considered both the standard deviation and the maximum variation between repeats in the triplicate (Figures 3a–3eiii), which are summarized in Table 1 and Supplementary Table S3, respectively. For the cell voltage at 1 A/cm^2, the in-house standard deviations ranged from 12 to 50 mV, while the maximum variations ranged from 88 to 118 mV. The HFR-corrected cell voltages had improved repeatability, with standard deviations of 16–44 mV and maximum variations of 29–108 mV. These differences demonstrated the difficulties of in-house repeatability in DI water testing, even when the same materials, protocol, and hardware were used in the same test station by the same operator.

Figure 4a shows the average BOT performance of all laboratories operating in DI water, with corresponding performance metrics summarized in Figure 4b; Table 1. EOT performance, after the short 2-h current hold at 1 A/cm^2, is reported in Supplementary Figure S8. From 13 tests across 5 sites, the full-cell voltage at 1 A/cm^2 ranged from 2.51 to 2.99 V, with an average value of 2.72 ± 0.17 V. The HFR values measured at 1 A/cm^2 spanned a broad range of 393–480 mΩ cm^2, with an average of 427 ± 37 mΩ cm^2. The corresponding ohmic losses are shown in Supplementary Figure S9. After correcting for HFR, the HFR-free voltages remained widely dispersed, ranging from 2.03 to 2.60 V, with a standard deviation of 195 mV (Figure 4b). The cross-lab differences in voltage at each current density are shown in Supplementary Figure S10. The cross-lab ΔV increased steadily with current density, rising from 221 mV at 0.1 A/cm^2 to 476 mV at 1 A/cm^2 for the full-cell voltage (Supplementary Table S3). A similar pattern was observed for the HFR-free voltage, whose cross-lab ΔV reached 563 mV at 1 A/cm^2. Overall, cross-lab reproducibility was significantly worse than in-house repeatability, as shown by a comparison of the maximum in-house and overall cross-lab standard deviations. The cross-lab standard deviations were 3.4x

and 4.4x higher for the cell voltage and HFR-free voltage at 1 A/cm^2, respectively. The higher deviation for the HFR-free cell voltage could be attributed to differences in EIS measurements across labs due to differences in potentiostat, cables, or component passivation/cell resistances. Further differences in EIS will be discussed in the discussion section.

A voltage loss breakdown analysis was used to determine the contributions of ohmic, kinetic, and mass transport (residual) losses to the cell voltage (Kreider et al., 2024). The details of this calculation, including the thermodynamic potential under different test conditions (Supplementary Table S4) and the Tafel analysis using the HFR-free voltage, are shown in the SI. Kinetic losses dominated the overall overpotential, ranging from 0.84 to 1.38 V across labs, with an average loss of 1.07 V at 1 A/cm^2 (Supplementary Figure S11). Calculating mass transport losses as the residual voltage, the average loss was only 30 mV at 1 A/cm^2. These trends demonstrated that both ohmic and kinetic contributions exhibited significant laboratory-to-laboratory variation under DI water operation. These differences were consistent with the sensitivity of DI water-fed AEMWE to membrane hydration, compression uniformity, electrolyte purity, and any trace impurities introduced from tubing, fittings, or recirculating reservoirs. Operation in DI water magnifies MEA-to-MEA differences and makes reproducibility particularly challenging. This sensitivity and strategies for improving reproducibility will be considered in the discussion section below.

4.2 KOH

AEMWE testing is also often performed with supporting electrolyte to improve performance and durability, and therefore the second half of this benchmarking effort focused on operation in supporting electrolyte. For this study, 0.1 M KOH was chosen to minimize corrosion of test station and cell hardware components, while being sufficiently concentrated at pH 13 to allow for reproducibility between labs and tests without undue influence from contaminants on conductivity. The MEA fabrication and test protocol were discussed in detail in the experimental section. Briefly, the anode was composed of a commercial Co_3O_4 catalyst layer with 0.78 ± 0.09 mg_{Co}/cm^2 loading and 10 wt% PiperION ionomer, supported on a Ni fiber PTL. The cathode was 0.27 ± 0.02 mg_{Pt}/cm^2 Pt/C with 30 wt% PiperION ionomer on a C GDL, and the membrane was 80 µm PiperION. Electrodes were fabricated at Lab 1 and distributed to the other labs, along with gaskets and membranes.

Figure 5 shows the BOT performance for the triplicate experiments run by each lab in 0.1 M KOH. The performance for each lab is further summarized in Table 2. In each triplicate measured within a single lab, significant performance variation was observed (Figures 5a–5e, i). To quantify in-house reproducibility, we considered the standard deviation and maximum variation between repeats in the triplicate (Figures 5a–5eiii). For the cell voltage at 1 A/cm^2, the standard deviation ranged from 9 to 28 mV, while the maximum voltage difference ranged from 18 to 60 mV (Supplementary Table S3). This was substantially higher than the ~5 mV in-house variation found for the previously reported PEMWE round robin, (Bender et al., 2019), up to a maximum of 11 mV at 2.5 A/cm^2, but significantly smaller than the variation found in DI water (118 mV). The HFR followed a general pattern of decreasing with increased current (Figures 5a–5eii); this has been attributed to a heating effect improving membrane conductivity (Ito et al., 2011). There was also significant in-house variation in the HFR, with the maximum difference across the triplicates ranging from 14 to 34 mΩ*cm^2. As with the PEMWE study (Bender et al., 2019), accounting for ohmic losses reduced the variation for some labs, while increasing the variation for others. At 1 A/cm^2, the in-house variation in HFR-free voltage ranged from 26 to 49 mV, with standard deviations of 13–20 mV (among the labs that completed three tests up to 1 A/cm^2). Thus, there was at least 4x higher in-house variation for AEMWE than for PEMWE. Potential causes for this in-house variability will be discussed in the next section.

Cross-lab variation was larger than the previously discussed in-house variations. From 14 tests across 5 labs, the average current density at 2 V was 1.66 ± 0.21 A/cm^2 and the average voltage at 1 A/cm^2 was 1.87 ± 0.03 V (Figure 6a). While an improvement over DI water, the performance lagged behind the US Department of Energy target of 2 A/cm^2 at 1.8 V for AEMWE (Satyapal, 2024). At 1 A/cm^2, the cross-lab difference in cell voltage between the highest and lowest performing labs was 88 mV (Figure 6b). This was 1.5x higher than the largest in-house variation (Supplementary Table S3). The standard deviation was 30 mV, comparable to the largest in-house variation. For the PEMWE round robin, albeit for only 7 tests across 3 labs, the cross-lab voltage difference was only 7 mV at 1 A/cm^2 and 27 mV at 2.5 A/cm^2 (Bender et al., 2019).

The HFR at 1 A/cm^2 was found to vary between the labs, from 102 to 139 mΩ cm^2, with an average of 127 ± 17 mΩ*cm^2 (Table 2). The ohmic losses due to HFR are shown in Supplementary Figure S12. The overall average HFR-free voltage at 1 A/cm^2 was 1.75 ± 0.03 V, indicating no change in standard deviation from the total cell voltage at 1 A/cm^2 (Figure 6b). The voltage difference plot shows very similar variation at 1 A/cm^2 for total cell and HFR-free voltage (Supplementary Figure S10), approximately 86 mV. This was 1.8x higher than the largest in-house variation for the HFR-free voltage. At low current densities, the HFR correction yielded lower variation, but this was reversed at high current densities. Using the HFR-free voltage, the kinetic losses were determined with a Tafel analysis. The average Tafel slope and exchange current density were 136 ± 13 mV/dec and 77 ± 46 µA/cm^2, respectively (Supplementary Table S5). These parameters were then used to calculate the kinetic loss as a function of current density (Supplementary Figure S13). At 1 A/cm^2, the kinetic losses varied from 483 to 525 mV across labs, for an average of 522 ± 22 mV. The average mass transport loss at 1 A/cm^2 was 40 mV, comparable to the value in DI water. The kinetics were thus still the largest contributor to the overpotential. Overall, both in-house and cross-lab variation were higher than was found in the PEMWE round robin, with HFR-correction accounting for only a small contribution to the variation, especially cross-labs. These findings will be discussed further in the next section.

Finally, 100-h chronopotentiometry (CP) measurements at 1 A/cm^2 were conducted to probe cross-lab differences in short-term durability. Only 3 labs participated in the durability measurement due to time limitations. As shown in Figure 7a, there was significant variation in the starting voltage for each lab. For both Lab 1 and 2, the initial voltages (1.77 and 1.83 V, respectively) were lower than the voltages found at 1 A/cm^2 from the polarization curves (Table 2). This seemingly improved performance between the polarization curve and the CP measurement is commonly found after testing

10.3389/fenrg.2026.1794912

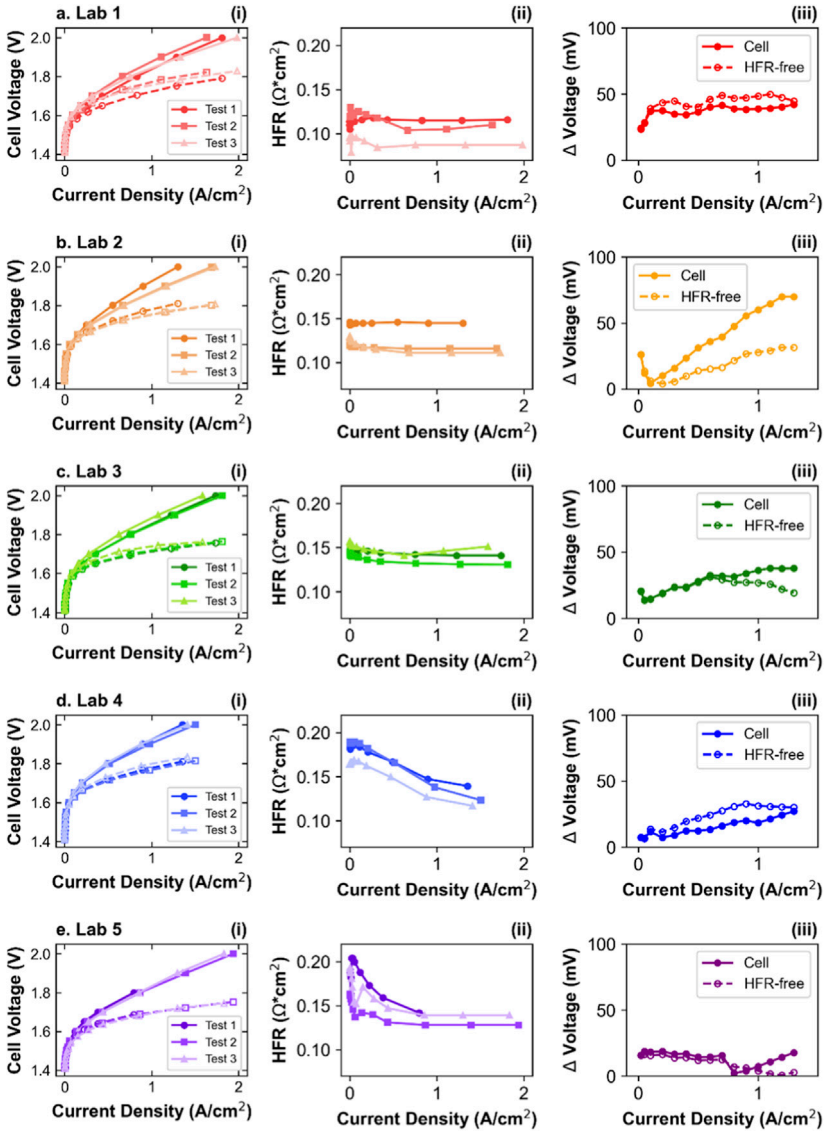

FIGURE 5
BOT performance in 0.1 M KOH. **(i)** Full cell voltage (solid lines) and HFR-free (dashed lines) polarization curves, **(ii)** HFR values, and **(iii)** maximum cell (solid lines) and HFR-free (dashed lines) voltage variation in the triplicate as a function of current density for **(a)** Lab 1 (red), **(b)** Lab 2 (gold), **(c)** Lab 3 (green), **(d)** Lab 4 (blue), **(e)** and Lab 5 (purple). Three tests were reported for each lab.

TABLE 2 **Performance summary in supporting electrolyte.**

Lab	1*	2*,†	3*	4*	5*,†,‡	Average^
Current at 2 V (A/cm^2)	1.81 ± 0.14	1.57 ± 0.19	1.71 ± 0.09	1.42 ± 0.06	1.89 ± 0.05	1.66 ± 0.20
Cell voltage at 1 A/cm^2 (V)	1.852 ± 0.017	1.886 ± 0.028	1.861 ± 0.016	1.917 ± 0.009	1.829 ± 0.004	1.87 ± 0.03
HFR at 1 A/cm^2 (mΩ*cm^2)	102 ± 12	124 ± 15	133 ± 6	136 ± 9	134 ± 6	127 ± 17
HFR-free voltage at 1 A/cm^2 (V)	1.750 ± 0.020	1.762 ± 0.013	1.722 ± 0.011	1.781 ± 0.013	1.695 ± 0.002	1.75 ± 0.03

*Values are reported as the mean and standard deviation of replicates from each lab.
^Values are reported as the mean and standard deviation of replicates from all labs.
†HFR calculated up to 1.8 V only.
‡Current measured only to 1.8 V for 1 replicate.

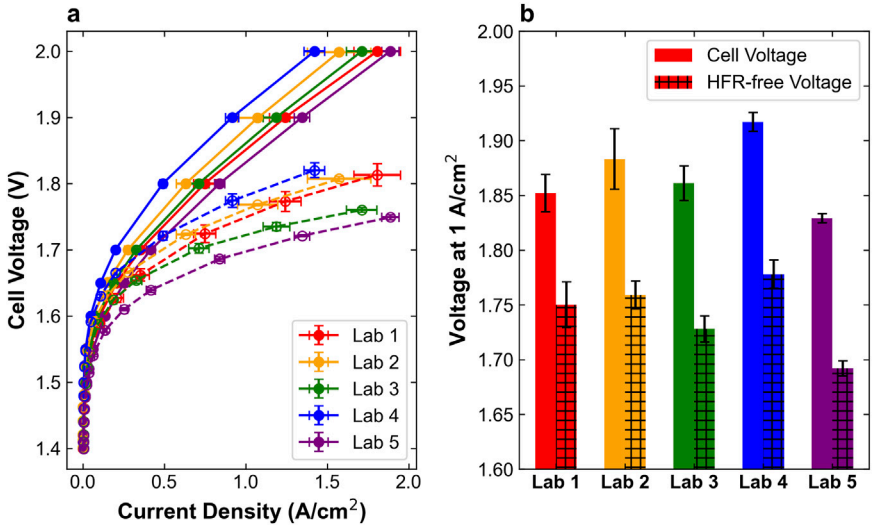

FIGURE 6
BOT performance in 0.1 M KOH. **(a)** Full (solid lines) and HFR-free (dashed lines) polarization curves. **(b)** Summary of full cell voltage (solid) and HFR-free (patterned) voltages at 1 A/cm^2. Colors: Lab 1 (red), Lab 2 (gold), Lab 3 (green), Lab 4 (blue), and Lab 5 (purple). Data were reported as the average and standard deviation of tests performed in triplicate.

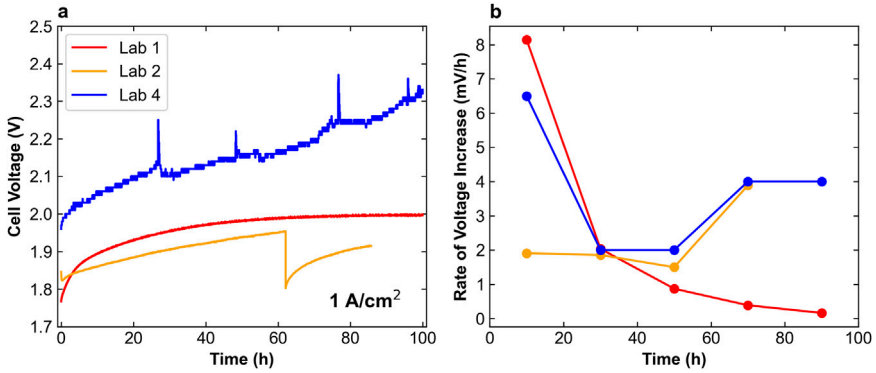

FIGURE 7
Short-term durability in 0.1 M KOH. **(a)** Chronopotentiometry measurements at 1 A/cm^2 for Lab 1 (red, 100 h), Lab 2 (gold, 84 h), and Lab 4 (blue, 100 h). **(b)** Summary of the rate of voltage increase for each test, taken as the average over 20 h periods (e.g., 0-20, 20-40, etc.).

is paused or the cell is exposed to open circuit voltage, which occurred before the CP measurement began (Blair et al., 2025). A similar phenomenon was demonstrated again during the CP for Lab 2, where the test restart at ~60 h resulted in a significant voltage decrease.

For AEMWE, precise definitions of break in and voltage loss rate have not been standardized. In general, the overall voltage loss rate is calculated from beginning to end of test, but additional insight can be gained from examining changes to the loss rate over time. With no test interruptions, Lab 1 had an overall voltage increase rate of 2.3 mV/h. The loss rate was not constant over time, decreasing from 3.7 mV/h in the first 60 h to 0.3 mV/h over the final 40 h (Figure 7b). Longer-term testing would be needed to verify that this is truly a "steady state" degradation rate. For Lab 2, the overall loss rates from 0 to 60 h and 60–80 h were 2.0 and 3.9 mV/h, respectively. Thus, while there was an initial recovery in performance after the interruption at 60 h, there was also a subsequent increase in degradation rate. Lab 4 had a similar profile to Lab 1 over the first 60 h, with a degradation rate of 3.5 mV/h, but then there was an acceleration in degradation to 4.0 mV/h after 60 h. Overall, we found similar degradation behavior over the first 60 h, but this diverged over the full length of the test.

5 Discussion

The round-robin tests showed significant variation both in-house and cross-lab (Supplementary Table S3), indicating that further iteration and validation of the protocol is required. An effort was made to control cross-lab variation by using the same cell hardware, membranes, and gaskets, and having one lab fabricate the MEAs. However, it was not possible to control all the differences in station design between labs. Furthermore, in-house variability may be introduced via cell assembly and non-uniformities in MEA

TABLE 3 Electrolyte properties.

Lab	1	2	3	4	5
KOH purity	86.8%	87.8%	89.6%	89.6%	89.6%
Fe content	≤0.0005%	≤0.001%	≤0.001%	≤0.001%	≤0.001%
K_2CO_3 content	0.3%	0.6%	0.85%	0.85%	0.85%
Water purity	Milli-Q	Deionized	Milli-Q	Milli-Q	Milli-Q
Flow rate (mL/min)	50	6*	100*	50	50
Volume (L)	3	1	6	1	5
Pre-heating	Coil heater	None	Coil heater	Hot plate	Immersion heater
N_2 blanket	400 sccm	n/a	n/a	n/a	n/a

*Flow rates deviated from the recommended protocol value of 50 mL/min, due to laboratory-specific setup limitations.

fabrication. Here, we discuss some likely causes of variability and propose solutions to improve reproducibility in AEMWE testing.

In round robin testing for PEMWE, temperature control was identified as a significant cause of the variability (Bender et al., 2019). At 1 A/cm^2, the voltage was found to increase by ~ 3 mV for every 1°C decrease in temperature. In this AEMWE round robin test, identical cell hardware was used for all tests. This ensured that the flow pattern and cell body heating (rod heaters inserted in the end plates) were held constant. However, the test stations outside of the cell were different from lab to lab. These differences included different electrolyte heating strategies, electrolyte flow rate, insulation of the electrolyte tubing, thermocouples, and PID controls. In particular, Lab 2 used a lower electrolyte flow rate and no electrolyte pre-heating, while the other labs pre-heated the electrolyte and used faster flow rates (Table 3). Analysis of the effects of temperature on AEMWE performance showed an even larger rate of ~10 mV increase per 1 °C decrease in temperature in DI water tests (Supplementary Figure S14). Thus, improving temperature control across laboratories could help to reduce variation. Additional temperature measurements at the inlet and outlets would provide insight into the effects of the different heating strategies.

In addition to heating, the cell hardware also affects compression and cell resistance. To minimize variability, multiple sets of cell hardware were prepared at a single site and distributed to all participating labs, and a consistent assembly protocol was used. However, the hardware used by each lab was distinct (not one set shared between labs), meaning that differences in contact resistance or compression were possible. Cell assembly may also be a source of error; even with experience, small variations in alignment or torque are possible and can affect performance. An approach for future round robin testing could be to have one lab distribute assembled cells. However, this can have additional complications with membrane dry out, freezing, or cell aging during transport. Realistically, efforts should be directed towards robust hardware designs and consistent assembly methods to minimize in-house variation. A comparison of performance using different commonly used or commercial cell designs would be beneficial for the field.

There were small differences in the MEAs, operating conditions, and protocols for testing in DI water and supporting electrolyte. These differences were in part based on inherent differences in the conditions, such as the improved stability of stainless steel in water or the higher HFR in DI water, motivating the use of thinner membranes. Furthermore, the protocols used reflect the standard procedures for two different labs, which diverge slightly due to different test stands, typical test types, and individual preference. Further work would be required to develop a full protocol and assess the impacts of the various choices that must be made (e.g., temperature, current vs. voltage control, activation procedure). Nevertheless, the results of testing under both conditions can be compared to understand the role of electrolyte in reproducibility. As expected, there were significant performance differences between DI water and 0.1 M KOH, with cell voltages at 1 A/cm^2 of 2.72 ± 0.17 and 1.87 ± 0.03 V, respectively. While the HFR was 3x higher in DI water, there was still a 550-mV difference in HFR-free voltage at 1 A/cm^2. This indicates a decrease in ohmic, kinetic, and transport losses with supporting electrolyte. In addition to improved performance, both the in-house and cross-lab variations were found to be lower in the supporting electrolyte (Supplementary Table S3). The in-house variations in cell and HFR-free voltage at 1 A/cm^2 were ~2x higher for DI water than for KOH. Accounting for HFR losses reduced the maximum in-house variation by 10%–20% for both electrolytes. The same analysis across labs showed significantly larger variation in DI water. This included a 5.4x higher variation in cell voltage at 1 A/cm^2 and 2.4x higher variation in HFR. This may partially reflect the intrinsic sensitivity of the cell in DI water. Under these conditions, fewer accessible active sites and the catalyst layer is more vulnerable to delamination. Beyond these differences, the preparation and contamination of the electrolyte is the most likely source of error.

The electrolyte, in particular pH and presence of contaminants, has previously been identified as a critical variable for AEMWE performance (Liu et al., 2021). For the tests in DI water, the electrolyte properties were likely affected by the source of water and contaminants from the electrolyte recirculation system, as well as any metal corrosion from the MEA or cell hardware. All labs used the same cell hardware and fittings, as well as the same test protocol, thus likely minimizing differences in the short-term corrosion. However, there were differences in electrolyte volume (1–6 L) and flow rate (6–50 mL/min) that could affect the concentration of contaminants (Table 3). Further, Lab 2 used deionized water, while all other labs used Milli-Q water; this was found to have a small effect on water resistivity, varying from 17.8 MΩ*cm for deionized to 18.2 MΩ*cm for Milli-Q. Most significantly, residual electrolyte and contaminants from previous tests were difficult to fully remove from the electrolyte recirculation systems, which was a possible cause of both in-house and cross-lab variability. Since the HFR decreased significantly as the pH increased, from an average of 427 mΩ*cm^2 in DI water to an average of 127 mΩ*cm^2 in 0.1 M KOH, differences in HFR between tests may provide insight into differences in

pH. For example, Lab 1 measured low HFR values, which may indicate higher levels of contamination from previous tests in supporting electrolyte. This highlights the need for rigorous cleaning methods between tests, with complete replacement of tubing and reservoirs as the only sure way to prevent cross-contamination. There were also challenges in consistent HFR calculation in this study due to differences in the potentiostats, EIS parameters, and inductance (Supplementary Figure S7). Efforts should be made to improve the quality of impedance spectra collected, as well as to standardize and report methods of HFR calculation (see SI for methods used in this work).

In the supporting electrolyte tests, the additional variable of the source and purity of KOH was introduced. Each lab used their own supply of KOH, resulting in the source varying across 3 vendors (Supplementary Table S1). While a consistent 0.1 M concentration was achieved by accounting for the different purity levels (87% vs. 90%), the KOH sources also varied slightly in levels of Fe and K_2CO_3. In PEMWE, metal contaminants such as Fe^{3+} and Ca^{2+} have shown detrimental effects on performance by decreasing the conductivity of the membrane, increasing the pH at the cathode, initiating the Fenton reaction, and leading to polymer degradation (Padgett et al., 2024; Becker et al., 2023). In alkaline conditions, however, Fe contaminants can incorporate into Ni- and Co-based OER catalysts and lead to improvements in activity (Appelhaus et al., 2024; Klaus et al., 2015; Burke et al., 2015; Trotochaud et al., 2014). In this study, changing from ≥85% to 100% pure KOH resulted in noticeably lower performance, including a 30-mV increase in voltage at 1 A/cm^2 (Supplementary Figure S15). Thus, these small variations in purity and Fe content may have contributed to the observed cross-lab variation. While low, the carbonate concentration in the KOH pellets could result in lowered electrolyte pH and substitution in the membrane, lowering the conductivity. Carbonation of the electrolyte is also possible with air exposure; Lab 1 used a N_2 blanket over the electrolyte to prevent CO_2 introduction during testing, but this was not used by the other labs. The station design will also affect the rate of water evaporation and changes in pH over time, which must be monitored. In future benchmarking efforts, the KOH source should be standardized, and the electrolyte pH/density should be verified prior to use. Monitoring pH, conductivity, and contaminants and correlation with HFR and performance over time would provide further insight into the role of the electrolyte.

Finally, we offer some recommendations to improve comparability in the field. First, a comparison with a baseline using standard commercial materials should be included whenever possible to validate the experimental set up. If the catalysts and membranes used in this effort are accessible, then direct comparison can be made from this baseline to the performance in DI water and 0.1 M KOH demonstrated here. If other commercial baselines are used, care should be taken that the baseline data are reasonable relative to literature. Consistent performance metrics are also needed to facilitate comparisons across the literature; at minimum, the HFR and cell voltage at 1 A/cm^2 should be reported. Since the HFR is sensitive to differences in pH, temperature, compression, and membrane properties that may exist between test setups, comparison of the HFR-free data can help to minimize the effects of these variables that are typically not the focus of the study. Differences in electrolyte will likely remain a source of error in the field; the vendor, purity, and lot number of the electrolyte should be reported to allow for identification of sources of variability. Efforts should also be made to measure and maintain consistent pH, as well as to clean test stations to avoid contaminant effects. Thorough reporting of these experimental details, as well as the station design, heating strategy, cell assembly, and test protocol will improve understanding of cross-lab differences and help to inform best practices for the field.

6 Conclusion

Here we have presented the results of a round-robin study between 5 laboratories of AEMWE testing in 0.1 M KOH and DI water. Baseline materials sets were chosen for testing based on commercial availability and material stability. Averaging across ~15 datasets, baseline performance metrics were reported in both electrolytes. Analysis of in-house variation indicated that differences in cell voltage and HFR were much higher than those reported from PEMWE round-robins, with variation increasing in DI water. The cross-lab variation was at least 1.5 times higher than the in-house, indicating that differences in test stations and protocols between labs exacerbated the variability. Improving temperature control and minimizing, or at least standardizing, contaminants in the electrolyte were identified as possible strategies to reduce variability and improve comparability across labs. To allow for improved comparisons in the field, several recommendations were made. First, studies should compare their results to a baseline test using commercial materials, ideally tested under identical conditions; results presented in this work may further be used as a reference for expected performance. Second, consistent performance metrics, such as HFR and cell voltage at 1 A/cm^2, should be reported for all tests. Finally, to facilitate improved understanding of how experimental factors affect performance, as much experimental information as possible should be reported for the test stations, electrolyte, and test protocols. As the field continues to grow, continued standardization through protocol development and identification of baseline materials will be critical to success.

Data availability statement

The original contributions presented in the study are included in the article/Supplementary Material, further inquiries can be directed to the corresponding author.

Author contributions

MK: Writing – review and editing, Investigation, Methodology, Conceptualization, Writing – original draft, Formal Analysis. MR: Writing – original draft, Formal Analysis, Writing – review and editing, Conceptualization, Methodology, Investigation. LB: Writing – review and editing, Methodology, Conceptualization, Investigation. DS: Investigation, Writing – review and editing. MK: Writing – review and editing, Methodology, Conceptualization, Investigation. PY: Writing – review and editing, Investigation. H-MJC: Supervision, Investigation, Writing – review and editing.

RH: Writing – review and editing, Investigation, Conceptualization. IR: Investigation, Writing – review and editing, Conceptualization. AE: Writing – review and editing, Investigation. NO: Investigation, Writing – review and editing. AN: Supervision, Writing – review and editing. SB: Supervision, Writing – review and editing. IZ: Supervision, Writing – review and editing. TJ: Supervision, Writing – review and editing. SA: Writing – review and editing, Conceptualization. BL: Writing – review and editing, Supervision, Conceptualization.

Funding

The author(s) declared that financial support was received for this work and/or its publication. This work was authored in part by the National Laboratory of the Rockies for the U.S. Department of Energy (DOE) under contract no. DE-AC36-08GO28308. Funding provided by the U.S. Department of Energy Office of Critical Minerals and Energy Innovation Alternative Fuels and Feedstocks Office. MR, IRA, ACN, and TFJ acknowledge support by the U.S. Department of Energy, Office of Science, Office of Basic Energy Sciences, Chemical Sciences, Geosciences, and Biosciences Division, Catalysis Science Program to the SUNCAT Center for Interface Science and Catalysis for electrolyzer set-up and measurements made at Stanford/SLAC. Partial support for research materials and hardware setup was provided by the Office of Naval Research, grant N00014-24-1-2433. MR acknowledges the Stanford Graduate Fellowship, RAISE Fellowship, and GEM Fellowship. IRA acknowledges the National Science Foundation Graduate Research Fellowship under grant number DGE-2146755. Versogen and University of California Berkeley acknowledge the funding provided by US-DOE-EERE under the collaborative award no. DE-EE0011322 through the sub-award agreement from University of California Berkeley.

Conflict of interest

Authors LB and BL were employed by Versogen. Author NO was employed by Nel Hydrogen.

The remaining author(s) declared that this work was conducted in the absence of any commercial or financial relationships that could be construed as a potential conflict of interest.

Generative AI statement

The author(s) declared that generative AI was not used in the creation of this manuscript.

Any alternative text (alt text) provided alongside figures in this article has been generated by Frontiers with the support of artificial intelligence and reasonable efforts have been made to ensure accuracy, including review by the authors wherever possible. If you identify any issues, please contact us.

Publisher's note

Author disclaimer

The views expressed in the article do not necessarily represent the views of the DOE or the U.S. Government. The U.S. Government retains and the publisher, by accepting the article for publication, acknowledges that the U.S. Government retains a nonexclusive, paid-up, irrevocable, worldwide license to publish or reproduce the published form of this work, or allow others to do so, for U.S. Government purposes.

Supplementary material

The Supplementary Material for this article can be found online at: https://www.frontiersin.org/articles/10.3389/fenrg.2026.1794912/full#supplementary-material

SUPPLEMENTARY TABLE 1
Pol Curves

SUPPLEMENTARY TABLE 2
DI Water EIS

SUPPLEMENTARY TABLE 3
KOH EIS

SUPPLEMENTARY DATA SHEET 1
Supplementary Materials

SUPPLEMENTARY DATA SHEET 2
KOH Summary

SUPPLEMENTARY DATA SHEET 3
Example Code

References

Appelhaus, S., Ritz, L., Pape, S.-V., Lohmann-Richters, F., Kraglund, M. R., Jensen, J. O., et al. (2024). Benchmarking performance: a round-robin testing for liquid alkaline electrolysis. *Int. J. Hydrog. Energy* 95, 1004–1010. doi:10.1016/j.ijhydene.2024.11.288

Ayers, K., Danilovic, N., Ouimet, R., Carmo, M., Pivovar, B., and Bornstein, M. (2019). Perspectives on low-temperature electrolysis and potential for renewable hydrogen at scale. *Annu. Rev. Chem. Biomol. Eng.* 10 (10), 219–239. doi:10.1146/annurev-chembioeng-060718-030241

Becker, H., Murawski, J., Shinde, D. V., Stephens, I. E. L., Hinds, G., and Smith, G. (2023). Impact of impurities on water electrolysis: a review. *Sustain. Energy Fuels* 7 (7), 1565–1603. doi:10.1039/D2SE01517J

Bender, G., Carmo, M., Smolinka, T., Gago, A., Danilovic, N., Mueller, M., et al. (2019). Initial approaches in benchmarking and round robin testing for proton exchange membrane water electrolyzers. *Int. J. Hydrog. Energy* 44 (18), 9174–9187. doi:10.1016/j.ijhydene.2019.02.074

Blair, S. J., Wrubel, J. A., Parrish, C., Parimuha, M. R., Foster, J., Pylypenko, S., et al. (2025). Reversible losses in proton exchange membrane water electrolysis. *J. Electrochem. Soc.* 172 (3), 034517. doi:10.1149/1945-7111/adc23f

Burke, M. S., Kast, M. G., Trotochaud, L., Smith, A. M., and Boettcher, S. W. (2015). Cobalt–iron (oxy)Hydroxide oxygen evolution electrocatalysts: the role of structure and composition on activity, stability, and mechanism. *J. Am. Chem. Soc.* 137 (10), 3638–3648. doi:10.1021/jacs.5b00281

Danilovic, N., Bender, G., and Weber, A. (2021). *H2NEW LTE: Performance and Benchmarking*.

Du, N., Roy, C., Peach, R., Turnbull, M., Thiele, S., and Bock, C. (2022). Anion-exchange membrane water electrolyzers. *Chem. Rev.* 122 (13), 11830–11895. doi:10.1021/acs.chemrev.1c00854

Ham, K., Hong, S., Kang, S., Cho, K., and Lee, J. (2021). Extensive active-site formation in trirutile CoSb2O6 by oxygen vacancy for oxygen evolution reaction in anion exchange membrane water splitting. *ACS Energy Lett.* 6 (2), 364–370. doi:10.1021/acsenergylett.0c02359

Hassan, N. U., Zheng, Y., Kohl, P. A., and Mustain, W. E. (2022). KOH vs deionized water operation in anion exchange membrane electrolyzers. *J. Electrochem. Soc.* 169 (4), 044526. doi:10.1149/1945-7111/ac5f1d

Hassan, N. U., Motyka, E., Kweder, J., Ganesan, P., Brechin, B., Zulevi, B., et al. (2023). Effect of porous transport layer properties on the anode electrode in anion exchange membrane electrolyzers. *J. Power Sources* 555, 232371. doi:10.1016/j.jpowsour.2022.232371

Huang, G., Mandal, M., Hassan, N. U., Groenhout, K., Dobbs, A., Mustain, W. E., et al. (2020). Ionomer optimization for water uptake and swelling in anion exchange membrane electrolyzer: Oxygen evolution electrode. *J. Electrochem. Soc.* 167 (16), 164514. doi:10.1149/1945-7111/abcde3

Ito, H., Maeda, T., Nakano, A., and Takenaka, H. (2011). Properties of nafion membranes under PEM water electrolysis conditions. *Int. J. Hydrog. Energy* 36 (17), 10527–10540. doi:10.1016/j.ijhydene.2011.05.127

Kim, I. T., Kim, S.-H., Ha, J. S., Kim, T. H., Cho, J., Park, G. D., et al. (2023). Oxygen deficient yolk–shell structured Co3O4 microspheres as an oxygen evolution reaction electrocatalyst for anion exchange membrane water electrolyzers. *J. Mater. Chem. A* 11 (31), 16578–16585. doi:10.1039/D3TA02710D

Klaus, S., Cai, Y., Louie, M. W., Trotochaud, L., and Bell, A. T. (2015). Effects of Fe electrolyte impurities on $Ni(OH)_2$/NiOOH structure and oxygen evolution activity. *J. Phys. Chem. C* 119 (13), 7243–7254. doi:10.1021/acs.jpcc.5b00105

Kreider, M. E., Yu, H., Osmieri, L., Parimuha, M. R., Reeves, K. S., Marin, D. H., et al. (2024). Understanding the effects of anode catalyst conductivity and loading on catalyst layer utilization and performance for anion exchange membrane water electrolysis. *ACS Catal.* 14 (14), 10806–10819. doi:10.1021/acscatal.4c02932

Lee, S. A., Kim, J., Kwon, K. C., Park, S. H., and Jang, H. W. (2022). Anion exchange membrane water electrolysis for sustainable large-scale hydrogen production. *Carbon Neutralization* 1 (1), 26–48. doi:10.1002/cnl2.9

Lim, J., Klein, J. M., Lee, S. G., Park, E. J., Kang, S. Y., Maurya, S., et al. (2024). Addressing the challenge of electrochemical ionomer oxidation in future anion exchange membrane water electrolyzers. *ACS Energy Lett.* 9 (6), 3074–3083. doi:10.1021/acsenergylett.4c00832

Liu, J., Kang, Z., Li, D., Pak, M., Alia, S. M., Fujimoto, C., et al. (2021). Elucidating the role of hydroxide electrolyte on anion-exchange-membrane water electrolyzer performance. *J. Electrochem. Soc.* 168 (5), 054522. doi:10.1149/1945-7111/ac0019

Meek, K. M., Antunes, C. M., Strasser, D., Owczarczyk, Z. R., Neyerlin, A., and Pivovar, B. S. (2019). High-throughput anion exchange membrane characterization at NREL. *ECS Trans.* 92 (8), 723–731. doi:10.1149/09208.0723ecst

Miller, H. A., Bouzek, K., Hnat, J., Loos, S., Bernäcker, C. I., Weißgärber, T., et al. (2020). Green hydrogen from anion exchange membrane water electrolysis: a review of recent developments in critical materials and operating conditions. *Sustain. Energy Fuels* 4 (5), 2114–2133. doi:10.1039/C9SE01240K

Padgett, E., Adesso, A., Yu, H., Wrubel, J., Bender, G., Pivovar, B., et al. (2024). Performance losses and current-driven recovery from cation contaminants in PEM water electrolysis. *J. Electrochem. Soc.* 171 (6), 064510. doi:10.1149/1945-7111/ad576b

Parimuha, M. R., Young, J. L., Lee, J. K., Yilmaz, A., Diaz-Abad, S., Gawas, R., et al. (2025). Proton exchange membrane electrolysis benchmarking: identifying and removing sources of variation in test stations, hardware, and membrane electrode assembly fabrication. *Int. J. Hydrog. Energy* 114, 486–496. doi:10.1016/j.ijhydene.2025.02.443

Park, Y. S., Kim, C., Lee, J., Jeong, J.-Y., Park, Y., Jang, M. J., et al. (2025). Oxygen-deficient Co3O4 electrode for anion exchange membrane water electrolyzer. *Int. J. Energy Res.* 2025 (1), 3025302. doi:10.1155/er/3025302

Rios Amador, I., Hannagan, R. T., Marin, D. H., Perryman, J. T., Rémy, C., Hubert, M. A., et al. (2023). Protocol for assembling and operating bipolar membrane water electrolyzers. *Star. Protoc.* 4 (4), 102606. doi:10.1016/j.xpro.2023.102606

Satyapal, S. (2024). *Hydrogen and Fuel Cell Technologies Office Multi-Year Program Plan*, 51.

Titheridge, L. J., and Marshall, A. T. (2024). The rationale for a standardized testing protocol for anion exchange membrane water electrolyzers. *ACS Energy Lett.* 9 (3), 1288–1294. doi:10.1021/acsenergylett.4c00239

Tomić, A. Z., Pivac, I., and Barbir, F. (2023). A review of testing procedures for proton exchange membrane electrolyzer degradation. *J. Power Sources* 557, 232569. doi:10.1016/j.jpowsour.2022.232569

Tricker, A. W., Lee, J. K., Shin, J. R., Danilovic, N., Weber, A. Z., and Peng, X. (2023). Design and operating principles for high-performing anion exchange membrane water electrolyzers. *J. Power Sources* 567, 232967. doi:10.1016/j.jpowsour.2023.232967

Tricker, A. W., Ertugrul, T. Y., Lee, J. K., Shin, J. R., Choi, W., Kushner, D. I., et al. (2024). Pathways toward efficient and durable anion exchange membrane water electrolyzers enabled by electro-active porous transport layers. *Adv. Energy Mater.* 14 (9), 2303629. doi:10.1002/aenm.202303629

Trotochaud, L., Young, S. L., Ranney, J. K., and Boettcher, S. W. (2014). Nickel–iron oxyhydroxide oxygen-evolution electrocatalysts: the role of intentional and incidental iron incorporation. *J. Am. Chem. Soc.* 136 (18), 6744–6753. doi:10.1021/ja502379c

Varcoe, J., R., Atanassov, P. ; R., Dekel, D. ; M., Herring, A. ; A., Hickner, M. ; A., Kohl, P. ; R., et al. (2014). Anion-exchange membranes in electrochemical energy systems. *Energy Environ. Sci.* 7 (10), 3135–3191. doi:10.1039/C4EE01303D

Volk, E. K., Kwon, S., and Alia, S. M. (2023). Catalytic activity and stability of non-platinum group metal oxides for the oxygen evolution reaction in anion exchange membrane electrolyzers. *J. Electrochem. Soc.* 170 (6), 064506. doi:10.1149/1945-7111/acd605

Wu, X., and Scott, K. (2011). CuxCo3−xO4 ($0 \leq x < 1$) nanoparticles for oxygen evolution in high performance alkaline exchange membrane water electrolysers. *J. Mater. Chem.* 21 (33), 12344–12351. doi:10.1039/C1JM11312G

Xu, Q., Zhang, L., Zhang, J., Wang, J., Hu, Y., Jiang, H., et al. (2022). Anion exchange membrane water electrolyzer: electrode design, lab-scaled testing system and performance evaluation. *EnergyChem* 4 (5), 100087. doi:10.1016/j.enchem.2022.100087

Yanagi, R., Yang, P., Tricker, A. W., Chen, Y., Scott, M. C., Berlinger, S. A., et al. (2025). Enhancing water and oxygen transport through electrode engineering for AEM water electrolyzers. *Joule* 9 (7), 102001. doi:10.1016/j.joule.2025.102001

Zeng, K., and Zhang, D. (2010). Recent progress in alkaline water electrolysis for hydrogen production and applications. *Prog. Energy Combust. Sci.* 36 (3), 307–326. doi:10.1016/j.pecs.2009.11.002

Zhang, L., Xu, Q., Hu, Y., Chen, L., and Jiang, H. (2023). Benchmarking the pH–Stability relationship of metal oxide anodes in anion exchange membrane water electrolysis. *ACS Sustain. Chem. Eng.* 11 (36), 13251–13259. doi:10.1021/acssuschemeng.3c01619